Brain Research 1678 (2018) 138–145

Contents lists available at ScienceDirect

Brain Research

journal homepage: www.elsevier.com/locate/bres

Research report

Investigating the efficacy of a combination Aβ-targeted treatment in a mouse model of Alzheimer's disease

Mingzhe Liu [a,b,1], Stefan Jevtic [a,b,1], Kelly Markham-Coultes [b], Nicholas P.K. Ellens [c,d,2], Meaghan A. O'Reilly [c,d], Kullervo Hynynen [c,d], Isabelle Aubert [a,b], JoAnne McLaurin [a,b,*]

[a] Department of Laboratory Medicine and Pathobiology, University of Toronto, Toronto, ON, Canada
[b] Hurvitz Brain Sciences Research Program, Biological Sciences, Sunnybrook Research Institute, Toronto, ON, Canada
[c] Department of Medical Biophysics, University of Toronto, Toronto, ON, Canada
[d] Physical Sciences, Sunnybrook Research Institute, Toronto, ON, Canada

ARTICLE INFO

Article history:
Received 25 July 2017
Received in revised form 28 September 2017
Accepted 15 October 2017
Available online 21 October 2017

Keywords:
Magnetic resonance imaging
Focused ultrasound
Alzheimer's disease
Amyloid
Antibody
scyllo-Inositol

ABSTRACT

Amyloid-beta peptide (Aβ) plays a critical role in the pathogenesis of Alzheimer's disease (AD). Here, we explored the use of a combination treatment to reduce amyloid load through microglial phagocytosis in a mouse model of AD. We hypothesized that using an initial treatment of magnetic resonance image guided focused ultrasound (MRIgFUS) to transiently increase the blood–brain barrier (BBB) permeability and enhance the delivery of an Aβ-antibody (BAM-10), followed by *scyllo*-inositol treatment would result in accelerated clearance. TgCRND8 mice expressing both Swedish (KM670/671NL) and Indiana (V717F) APP mutations under the hamster prion (PrP) promoter at 5 months of age were either treated with *scyllo*-inositol or received an initial MRIgFUS treatment delivering BAM-10 prior to *scyllo*-inositol treatment for one month. Treated animals and untreated TgCRND8 littermates were then sacrificed at 6 months of age, and their brains were processed for immunohistochemistry and immunofluorescence. Amyloid load was quantified and analyzed through immunohistochemical staining. Astrocyte and microglial activation were quantified and analyzed through immunofluorescent staining. We found that both the *scyllo*-inositol treatment and combination treatment, MRIgFUS/BAM10+*scyllo*-inositol, significantly reduced amyloid load and astrocyte activation in the hippocampus and the cortex. Furthermore, in both treatment paradigms microglial activation and phagocytosis was increased in comparison to the untreated mice. There were no differences detected between the two treatment paradigms. We propose that the 30-day *scyllo*-inositol treatment saturated the early benefit of the MRIgFUS/BAM-10 treatment. In the future, multiple FUS treatments combined with BAM-10 throughout the duration of *scyllo*-inositol treatment may lead to more effective amyloid clearance.

1. Introduction

Alzheimer's Disease (AD) is a prominent neurodegenerative disease in the elderly population, with increased risk from aging (Selkoe, 2001). AD is characterized by the presence of amyloid-beta peptide (Aβ) plaques and neurofibrillary tangles in the brain, severe cognitive deficits and ultimately death (Reitz and Mayeux, 2014). The amyloid hypothesis proposes that the dysregulation of Aβ levels in the brain is the initiating step in AD pathogenesis (Hardy and Selkoe, 2002; Tarasoff-Conway et al., 2015). Despite numerous clinical trials targeted at increasing clearance and/or inhibiting Aβ production, there is currently no treatment available that slows or halts disease progression (Liu et al., 2017). Multiple studies, in rodent models of AD, have shown benefits from several treatment paradigms, including small-molecule therapy and passive immunization (Jordão et al., 2010; Ma et al., 2012; McLaurin et al., 2006, 2000; Weiner and Frenkel, 2006). These treatments have shown a significant reduction in Aβ peptide levels within

Abbreviations: Aβ, Amyloid-beta peptide; AD, Alzheimer's disease; BBB, Blood-Brain Barrier; CNS, Central nervous system; GFAP, Glial fibrillary acidic protein; MRI, Magnetic resonance image; MRIgFUS, Magnetic resonance image guided focused ultrasound; SI, *scyllo*-Inositol; SMIT1, Sodium/*myo*-inositol transporter 1; SMIT2, Sodium/*myo*-inositol transporter 1.

* Corresponding author at: Sunnybrook Research Institute, 2075 Bayview Avenue, Rm S113, Toronto, ON M4N 3M5, Canada.
E-mail address: jmclaurin@sri.utoronto.ca (J. McLaurin).

[1] Authors contributed equally towards completion of study.

[2] Present address: Department of Radiology, Johns Hopkins University, Baltimore, MD, USA.

https://doi.org/10.1016/j.brainres.2017.10.015
0006-8993/

the brain and a rescue of cognitive deficits (Jordão et al., 2010; Ma et al., 2012; McLaurin et al., 2006, 2000; Weiner and Frenkel, 2006).

At present, there are a number of passive immunization strategies in development for AD, with many of these focused on the development of antibodies against Aβ. Although several of these antibodies such as AAB-001 (Bapineuzumab) and LY-2062430 (Solanezumab) completed phase 3 clinical trials, none have shown improvement in primary cognitive outcomes in patients (Doody et al., 2014; Salloway et al., 2014). One drawback to passive immunization against Aβ in both human and animal models is the limited access of antibodies to the brain due to the blood-brain barrier (BBB). The majority of the anti-Aβ antibodies administered peripherally remains in the blood stream, with only 0.1% of antibodies crossing the intact BBB and entering the brain (Banks et al., 2002).

Magnetic resonance image (MRI)-guided focused ultrasound (MRIgFUS) technology was discovered over 25 years ago and originally utilization of MRIgFUS focused on thermal ablation, with a high intensity focused ultrasound wave (Hynynen, 2010). More recent studies have used MRI coupled with low-intensity focused ultrasound and microbubbles, within the blood stream, to transiently increases the permeability of the BBB, allowing for the delivery of therapeutic agents, such as antibodies, gene vectors, stem cells and nanoparticles (Burgess et al., 2011; Diaz et al., 2014; Hynynen et al., 2001; Jordão et al., 2010; Thévenot et al., 2012). In preclinical studies, MRIgFUS increased localized delivery of agents across the BBB through increased transcytosis, channel formation, and widened tight junctions (Sheikov et al., 2008; 2004). Furthermore, the permeability of BBB was restored in as little as 6 h post-FUS (Hynynen et al., 2006). The use of MRIgFUS for the targeted delivery of BAM-10, an antibody against Aβ, showed significant clearance of brain Aβ in a mouse model of AD (Jordão et al., 2010). BAM-10 is directed against residues 1–10 at the N-terminus of Aβ and treatment has shown efficiency in dissociating Aβ aggregates (Frenkel et al., 1998; McLaurin et al., 2002). Furthermore, cognitive deficits were rescued after BAM-10 treatment in the Tg2576 mouse model of AD (Kotilinek et al., 2002). Due to the success of MRIgFUS treatment alone and in conjunction with therapeutic agents in reducing amyloid load, activating microglia, by safely and temporarily opening the BBB in preclinical rodent models, phase 1 trials are currently underway to determine the safety and feasibility in AD patients (Meng et al., 2017).

Many small-molecules have been developed that also inhibit formation of Aβ oligomers and amyloid plaques (Nie et al., 2011). One such molecule is *scyllo*-inositol, a cyclohexanehexol that binds to Aβ peptides and inhibits further aggregation (McLaurin et al., 2006). In murine models, *scyllo*-inositol administration decreased plaque burden and inflammation, leading to improved cognitive performance (Aytan et al., 2013; Hawkes et al., 2010; McLaurin et al., 2006). *scyllo*-Inositol is actively transported into the brain through sodium/*myo*-inositol transporters 1 and 2 (SMIT1, SMIT2), which are expressed throughout the brain (Fenili et al., 2011). Moreover, SMIT1 and SMIT2 expression in the brain remains stable throughout aging in non-transgenic mice and increasing Aβ pathology in a mouse model of AD (Fenili et al., 2011). Similar to immunization strategies, the primary clinical outcomes for cognition were not met in patients treated with *scyllo*-inositol in a Phase 2 trial (Salloway, 2011).

MRIgFUS treatment alone has demonstrated beneficial effects in transgenic rodent models of AD. After MRIgFUS treatment, endogenous mouse antibodies were detected within cortical brain regions and activated microglial cells with enhanced phagocytosis were observed within 4 days of treatment (Jordão et al., 2013). Since both antibody- and *scyllo*-inositol- driven clearance of Aβ are partially reliant on microglial phagocytosis and degradation (Hawkes et al., 2012; Jordão et al., 2013), we hypothesized that a single treatment with MRIgFUS delivery of an Aβ-antibody would activate and boost microglial phagocytosis such that subsequent removal of Aβ with *scyllo*-inositol treatment would be accelerated in comparison to *scyllo*-inositol treatment alone. The choice of antibody was driven by the ability to increase Aβ degradation by microglial cells after delivery using MRIgFUS, thus BAM-10 was chosen (Bard et al., 2003; Morgan and Gitter 2004)

2. Results

We studied the effects of *scyllo*-inositol treatment alone and MRIgFUS/BAM10/*scyllo*-inositol (SI) combination treatment in TgCRND8 mice at an age that modelled mid AD-like pathology (5 months of age). Starting at 5 months of age, TgCRND8 mice received one MRIgFUS/BAM10 treatment, targeting 3 foci per cortex, bilaterally, followed by 1 month of *scyllo*-inositol treatment (n = 6), or *scyllo*-inositol treatment alone for one month (n = 6), along with age-matched untreated TgCRND8 controls (n = 6) (Fig. 1). No side-effects were observed and body weights were similar across treatment groups.

We investigated the effectiveness of single and combination therapeutic treatment on the reduction of amyloid load, activation of astrocytes and microglia in comparison to untreated TgCRND8 mice through immunochemistry and immunofluorescence staining of sections spanning the brain. We also examined the effects of both treatment paradigms on microglial phagocytosis of amyloid plaques. An MRIgFUS-BAM10 group alone was not included as we believed that previous work sufficiently demonstrated the effects of MRIgFUS/ BAM-10 in reducing amyloid load in TgCRND8 mice (Jordão et al., 2010). Furthermore, other studies have also reported the effect of MRIgFUS or Scanning Ultrasound (SUS) alone in TgAD mice on the reduction of amyloid (Burgess et al., 2014; Jordão et al., 2013; Leinenga and Gotz, 2015) as well as a rabbit model of amyloidosis (Alecou et al., 2017).

3. Reduction of amyloid load in both *scyllo*-inositol and combination treatments

The formation of Aβ plaques is a dynamic process that involves the aggregation of Aβ peptides that lead to amyloid plaque formation and deposition (Ahmed et al., 2010). Previous studies have shown *scyllo*-inositol treatment to inhibit the formation of fibrils and stabilize non-toxic oligomeric forms of Aβ, resulting in decreased plaque load in TgCRND8 mouse models (Ma et al., 2012; McLaurin et al., 2006; Salloway, 2011). Two month treatment with *scyllo*-inositol in 5 month old TgCRND8 mice significantly reduced the number of plaques as well as percent brain area covered in plaques (Fenili et al., 2007). Previous studies with a single MRIgFUS treatment combined with BAM-10 antibody in 4 month-old TgCRND8 mice significantly decreased size and number of Aβ cortical plaques in the FUS-targeted compared to the non-targeted hemisphere (Jordão et al., 2013, 2010). In the present study, plaque load within the hippocampus and cortex were examined as a function of treatment. In the hippocampus, *scyllo*-inositol treatment significantly reduced plaque load by 68% (38 ± 7 vs 116 ± 28, p = .02), while combination treatment significantly reduced plaque load by 66% (39 ± 4 vs 116 ± 28, p = .02) when compared to the untreated TgCRND8-mice (Fig. 2A). This significant reduction was also evident in the cortex, where *scyllo*-inositol treatment reduced plaque load by 45% (692 ± 51 vs 1263 ± 130, p = .001) and combination treatment decreased plaque load by 53% (596 ± 34 vs 1263 ± 130, p < .001) when compared to the untreated TgCRND8 mice (Fig. 2B). There was no statistical difference in both the

Fig. 1. Timeline of Therapeutic Interventions. TgCRND8 mice were treated or untreated at 5 months of age until sacrifice at 6-month. TgCRND8 mice were either treated with a single treatment of MRIgFUS with peripherally administered BAM-10 antibody directed to Aβ followed by *scyllo*-inositol (SI) treatment (MRIgFUS/BAM10/SI) or *scyllo*-inositol treatment alone for 30-days.

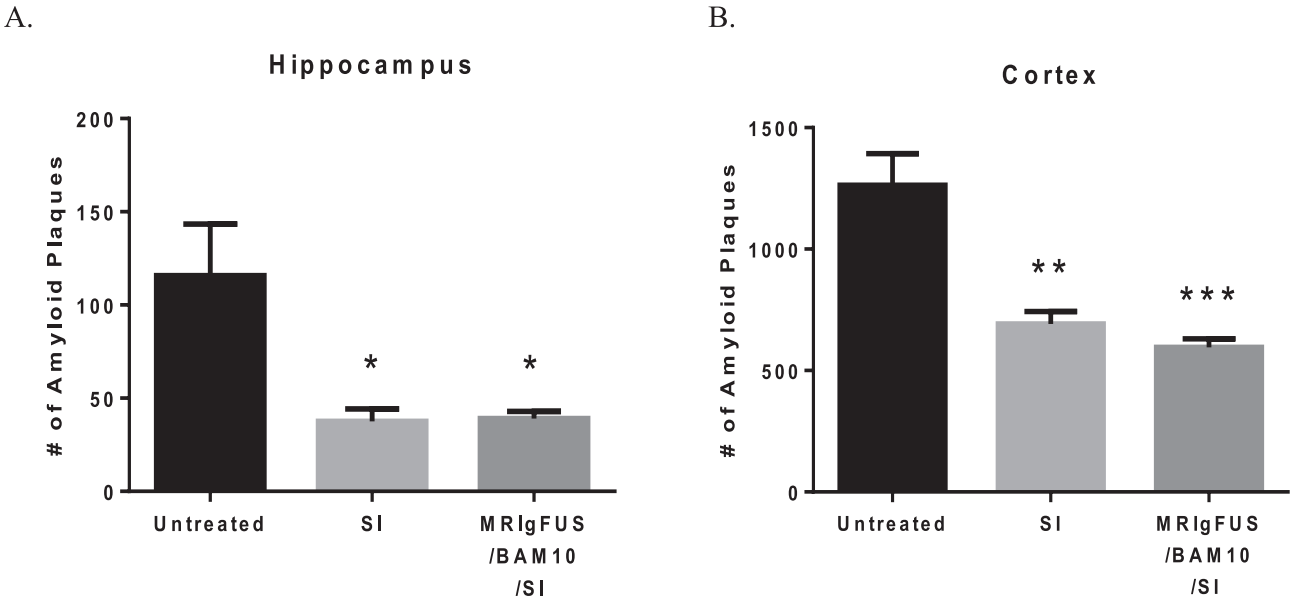

Fig. 2. Hippocampal and cortical Aβ plaques in *scyllo*-inositol treated, MRIgFUS/BAM10/SI treated and untreated TgCRND8 mice. Number of amyloid plaques found in the hippocampus (A), and in the cortex (B) are reduced after *scyllo*-inositol treatment and MRIgFUS/BAM10/SI treatment. Data presented as mean ± SEM, One-way ANOVA with Tukey's multiple comparisons test, $\alpha = 0.05$, * $p < .05$, ** $p < .01$, *** $p < .001$.

hippocampal and the cortical plaque load between *scyllo*-inositol and combination treatment ($p = .998$, $p = .7$, respectively).

4. Astrocyte activation reduction after *scyllo*-inositol and combination therapy

Astrocytes are the main type of glial cells present in the central nervous system, and play an important role in shaping the microarchitecture of the brain (Rodriguez et al., 2009). In the AD brain, the formation of Aβ plaques leads to the activation of astrocytes, reactive gliosis, and inflammation (Pekny et al., 2016). To examine the effectiveness of *scyllo*-inositol and combination treatment paradigms, we examined Aβ-related activation of $GFAP^+$ astrocytes. Previously, *scyllo*-inositol treatment alone significantly reduced astrogliosis throughout the hippocampus and the cortex in TgCRND8 mouse brain at 6 months of age[8]. However, in studies with MRIgFUS on 4 month old TgCRND8 mice, astrocyte activation has been shown to significantly increase within the first 4 days after the initial treatment when comparing treated and untreated cortices, and appear to decline by 15 days post treatment (Jordão et al., 2013). In the present study, the hippocampus and cortex were examined independently for the percentage of the brain covered by activated astrocytes in *scyllo*-inositol, combination treatment and untreated TgCRND8 mice (Fig. 3A). In agreement with a reduction in amyloid load within the hippocampus, there was a significant decrease in astrocyte coverage in both the *scyllo*-inositol (17 ± 3%) and combination treatment (20 ± 3%) when compared to the untreated TgCRND8 mice (33 ± 3%) ($p = .006$, $p = .03$, respectively Fig. 3B). This decrease was also observed in the cortex, whereby *scyllo*-inositol (7 ± 0.9%) and combination treatment (6 ± 0.6%) significantly reduced astrogliosis when compared to the untreated TgCRND8 mice (14 ± 2%) ($p = .001$, $p < .001$, respectively Fig. 3C). Again, no significant differences were observed between the two treatment paradigms in both the hippocampus and cortex ($p = .68$, $p = .7$, respectively).

5. Increased activated microglial and phagocytosis

Microglia are innate immune cells that are widely distributed throughout the brain, and play a crucial role in the clearance of Aβ plaques (Condello et al., 2015) (Fig. 4A). To examine whether the reduction of Aβ plaques is a function of microglial phagocytosis, we examined changes in microglia cell volume as a function of treatment. Changes in microglial cell size and number can be indicative of activation, as evidenced by increased cell surface area following therapeutic interventions (Jordão et al., 2013). To this end, microglia surrounding plaques in the *scyllo*-inositol, combination treatment and untreated TgCRND8 mouse cortex and hip-

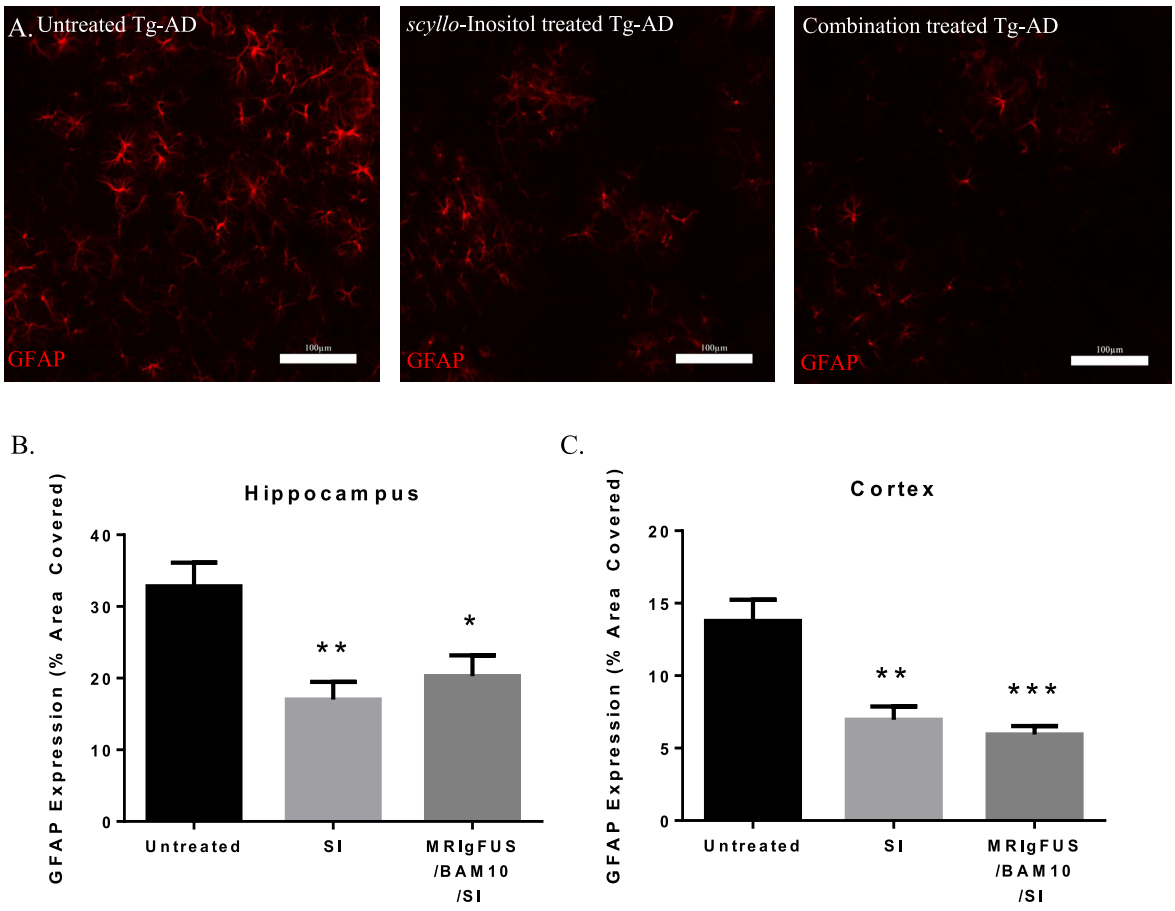

Fig. 3. Astrocyte activation in *scyllo*-inositol treated, MRIgFUS/BAM10/SI treated and untreated TgCRND8 mice. (A) Immunofluorescent images of GFAP immunoreactivity in the cortex of untreated, *scyllo*-inositol, and MRIgFUS/BAM10/SI treated mice. Percentage of GFAP immunoreactivity in the hippocampus (B), and in the cortex (C), are reduced after *scyllo*-inositol treatment and MRIgFUS/BAM10/SI treatment. Data presented as mean ± SEM, One-way ANOVA with Tukey's multiple comparisons test, $\alpha = 0.05$, * represents $p < .05$, ** represents $p < .01$, *** represents $p < .001$.

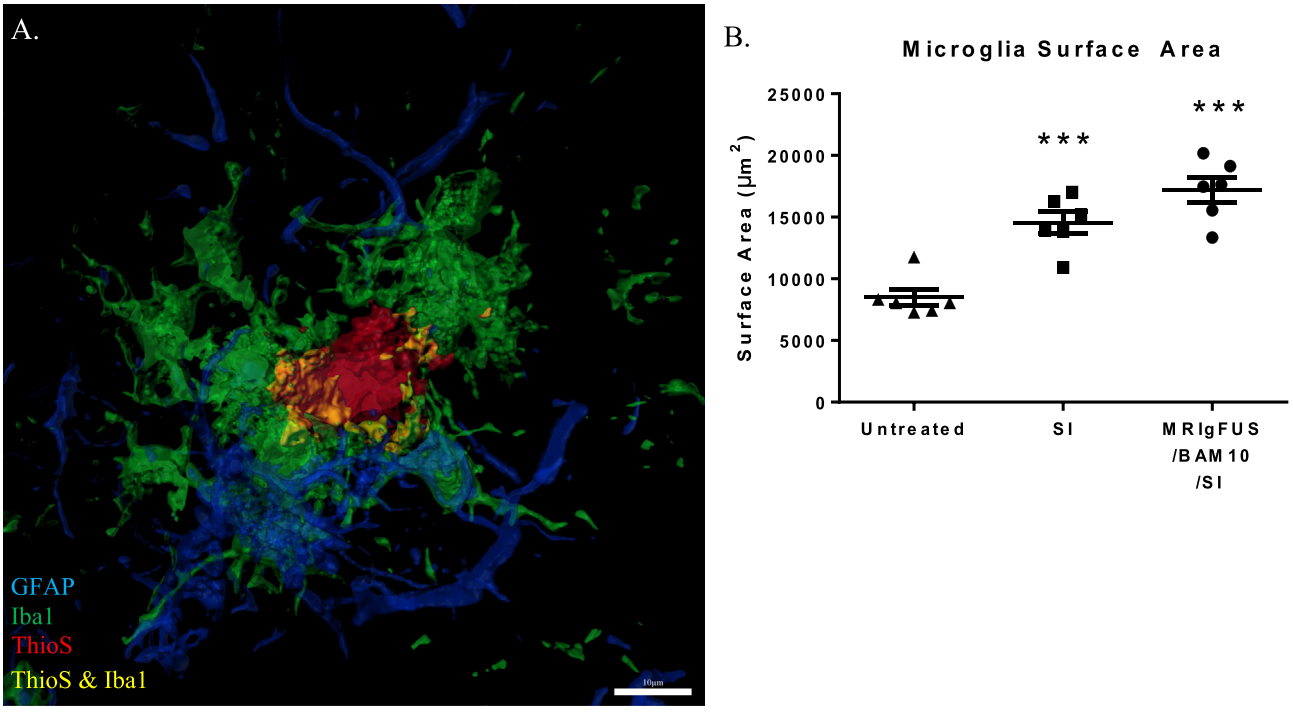

Fig. 4. Microglial activation in *scyllo*-inositol treated, MRIgFUS/BAM10/SI treated and untreated TgCRND8 mice. (A) 3D IMARIS rendering of a triple stain for astrocyte (GFAP, blue), microglia (Iba1, green) and amyloid plaque (ThioS, red), with colocalization of amyloid and microglia in yellow. (B) Microglia surface area is increased after *scyllo*-inositol and MRIgFUS/BAM10/SI treatment. Data presented as mean ± SEM, One-way ANOVA with Tukey's multiple comparisons test, $\alpha = 0.05$, *** represents $p < .001$.

pocampus were randomly sampled and analyzed. In the *scyllo*-inositol treated group, there was a significant increase in microglial surface area (14534 ± 892 μm^2) when compared to untreated group (8485 ± 677 μm^2) ($p < .001$, Fig. 4B). Similarly, in the combination treated group, there was an increase in microglial activation (17216 ± 1007 μm^2) when compared to the untreated cortex ($p < .001$, Fig. 4B). However, no significant differences were detected between the treatment groups ($p = .11$).

To determine whether microglia actively phagocytosed Aβ/amyloid in contrast to surrounding Aβ/amyloid plaques to function as a barrier, we investigated the co-localization of Aβ within microglial cells (Fig. 5A-C). After *scyllo*-inositol treatment, there was a significant increase in the percent of Aβ phagocytosed within microglia (23 ± 4% vs 12 ± 2%) in comparison to the untreated group ($p = .048$, Fig. 5D). Similarly, the combination treated group (21 ± 3% vs 12 ± 2%) showed a trend towards an increase in Aβ phagocytosis when compared to the untreated group ($p = .1$, Fig. 5D). Overall, both *scyllo*-inositol and combination treatments increased microglial activation around Aβ plaques, and increased Aβ internalization within microglial cells.

6. Discussion

In this study, we investigated the potential synergistic effects of a combination therapy between two Aβ lowering strategies, one with high central nervous system (CNS) bioavailability and the other with enhanced activation of endogenous clearance mechanisms (Jordão et al., 2013; McLaurin et al., 2006). The work was driven by the idea that a single treatment with MRIgFUS in combination with an anti-Aβ antibody, BAM10, would prime

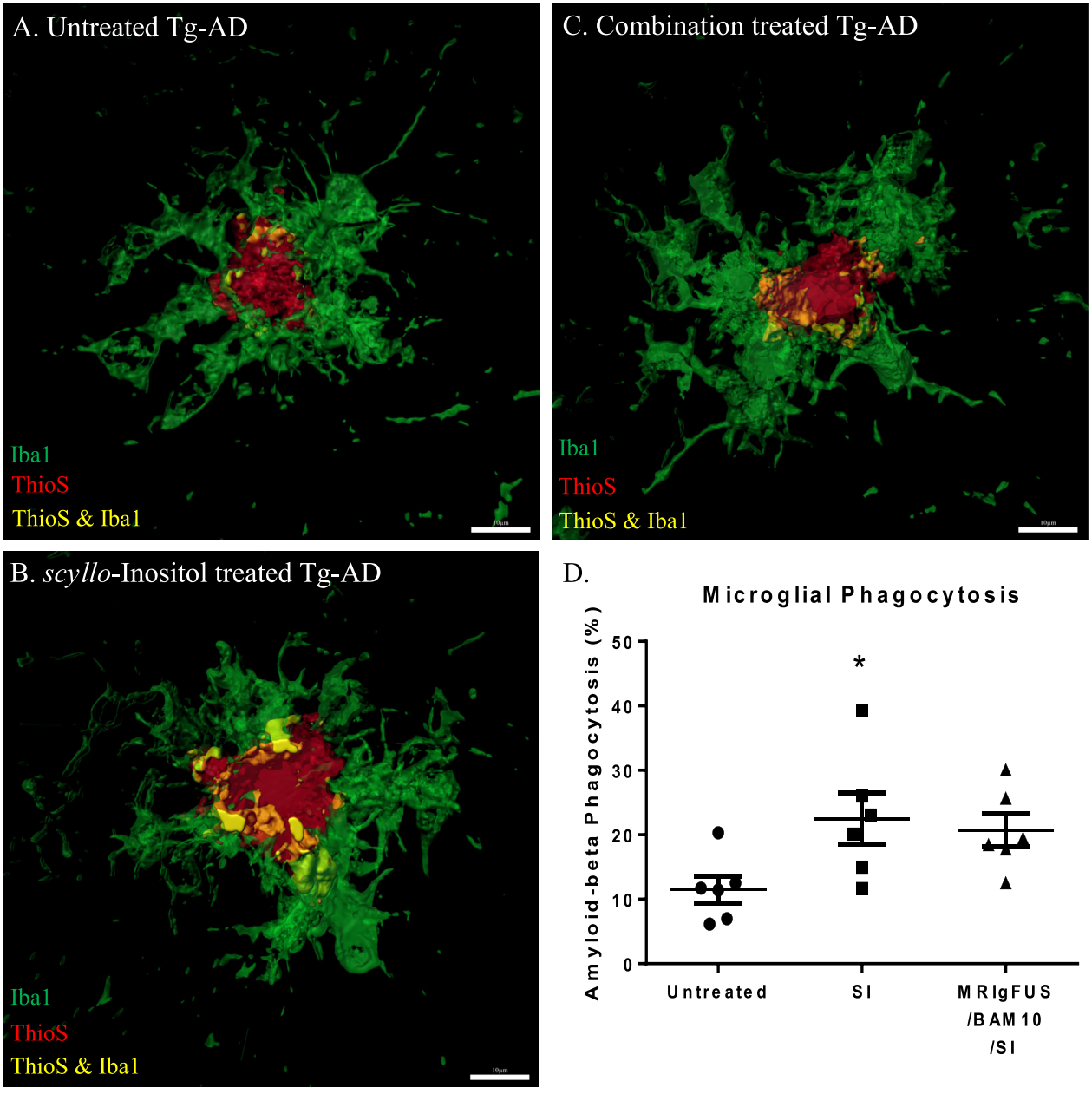

Fig. 5. Microglial phagocytosis in *scyllo*-inositol treated, MRIgFUS/BAM10/SI treated and untreated TgCRND8 mice. (A) 3D IMARIS rendering of a double stain for microglia (Iba1) and amyloid plaques (ThioS) of an untreated (B), *scyllo*-inositol treated and (C) MRIgFUS/BAM10/SI treated TgCRND8 mouse hippocampus. (D) Microglia phagocytosis was significantly increased after *scyllo*-inositol treatment and showed a strong increasing trend in MRIgFUS/BAM10/SI treatment. Data presented as mean ± SEM, One-way ANOVA with Tukey's multiple comparisons test, $\alpha = 0.05$, * represents $p < .05$.

microglial cells into active phagocytes and thus either synergistically or additively increase the *scyllo*-inositol induced clearance of Aβ over time. This hypothesis was based on the preclinical studies in a TgAD mouse model that demonstrated MRIgFUS + BAM10 reduced amyloid plaques and MRIgFUS alone increased microglial activation 4 days after treatment and resolved after 15 days (Jordão et al., 2013; 2010). Furthermore, BAM-10 as well as endogenous mouse IgG and IgM were detectable within the brain 4 days post FUS treatment (Jordão et al., 2013; 2010). Thus, these previous studies suggested that priming of microglia into active phagocytes was not sustained. We then hypothesized that the primed phagocytes would be more efficient in removing *scyllo*-inositol-Aβ complexes to decrease amyloid plaque load. Preclinical studies with *scyllo*-inositol demonstrated that steady state levels were achieved within 5 days of treatment (Fenili et al., 2007), thus optimal drug dose would be achieved within the window of MRIgFUS/BAM-10 efficacy. Our results demonstrate a trend to increased surface area covered in microglia within the cortex in the MRIgFUS/BAM-10/SI treatment in comparison to the *scyllo*-inositol treatment. However, the reduction in amyloid plaques and the amount of amyloid that was detected within microglial cells were not statistically different between the two treatment groups. This apparent discrepancy may be attributed to the difference in mechanism of action of BAM-10 and *scyllo*-inositol. BAM-10 specifically targets the amyloid plaques and thus drives direct clearance by plaque associated microglia (Kotilinek et al., 2002; Lai and McLaurin, 2012), whereas *scyllo*-inositol binds to and stabilizes small soluble conformers of Aβ that are phagocytosed by both plaque associated and non-plaque associated microglia (Hawkes et al., 2012; McLaurin et al., 2006). Furthermore, our study showed a difference in treatment effect when compared to that of the initial MRIgFUS+BAM10 studies (Jordão et al., 2010). Due to the differences in FUS parameters, number of foci targeted, age of the TgCRND8 mice receiving treatment, and the differences in the region of interest analyzed, these two studies cannot be directly compared. However, we believe that these two results are supportive of utilizing MRIgFUS for the reduction in amyloid, whether as a function of BAM10 or combination therapy.

As previously proposed, the reduction in astrogliosis that was detected in both the MRIgFUS/BAM-10/SI and *scyllo*-inositol treatment groups in comparison to untreated TgCRND8 mice, is the direct result of decreased Aβ load, as they were not statistically different.

Previous studies have shown that *scyllo*-Inositol treatment or BAM-10 treatment alone significantly improve cognitive outcomes in Tg-AD mice and that performance was not significantly different from non-transgenic littermates (Kotilinek et al., 2002; McLaurin et al., 2006). With regards to spatial memory, after 1 month of *scyllo*-Inositol treatment, no significant differences were found in cognitive performance between 6 months old TgCRND8 mice and their nontransgenic littermates (Hawkes et al., 2012; McLaurin et al., 2006). Furthermore, MRIgFUS treatment in TgAD mice showed improvements in hippocampal dependent memory in comparison to untreated TgAD mice and were not statistically different from treated non-transgenic littermates (Burgess et al., 2014). Taken altogether, given that both MRIgFUS and *scyllo*-Inositol treatment alone returned cognitive function of TgAD mice to levels of their nontransgenic littermates and due to the limitation of examining behavioural phenotypes in TgAD mice, we chose not to incorporate a behavioral arm in our studies.

7. Conclusions

In light of the current results, we propose that the 30-day treatment with *scyllo*-inositol saturated the potential benefit of the MRIgFUS/BAM-10 treatment. MRIgFUS is likely to increase treatment efficacy the most for therapeutics with poor CNS bioavailability. In the future, we propose that repeated FUS treatments in combination with immunotherapy and *scyllo*-inositol may result in more effective amyloid clearance. Treatment strategies with high CNS bioavailability including *scyllo*-inositol, will benefit from better patient selection and earlier intervention times.

8. Methods and materials

8.1. Mice

Sex-balanced 5-month old TgCRND8 mice (n = 18) expressing both Swedish (KM670/671NL) and Indiana (V717F) APP mutations under the hamster prion (PrP) promoter and maintained on a C3H/C57BL6 background were used for this study. After treatment, mice were perfused with phosphate-buffered saline and 4% paraformaldehyde (PFA). Brains were removed, and post-fixed in 4% PFA overnight, prior to 30% sucrose solution for tissue preservation. Coronal brain sections were obtained using a freezing microtome at 40 μm and stored in tissue collecting solution at −20 °C until use. All animal procedures were conducted with approval from the Animal Care Committee of Sunnybrook Research Institute, and in accordance with the Canadian Council on Animal Care.

8.2. MRI-guided FUS delivery

Mice were anesthetized using 2% isofluorane and medical air, and secured in the supine position on a small animal MRIgFUS compatible positioning system (Chopra et al., 2009; Ellens et al., 2015). MR imaging was performed at 7T Bio-Spec 70/30 USR (Bruker, Billerica, MA). MRI gadolinium contrast agent (0.2 ml/kg, Omniscan, 574 Da, GE Healthcare) and FUS microbubble contrast agent (0.04 ml/kg, Definity), and BAM-10 (1 mg/kg, Sigma A3981) were administered through a tail vein catheter simultaneously with the start of the ultrasound treatment. Focused ultrasound (10 ms bursts, 1Hz repetition rate) was targeted to 3 foci per cortex and treated bilaterally for a total of 2 min. The acoustic pressure was actively controlled on a burst-to-burst basis based on the analysis of microbubble signal recorded during each burst, as has been previously described (O'Reilly and Hynynen, 2012). The FUS transducer had a 7.5 mm diameter aperture, 6 cm radius of curvature and a frequency of 0.5515 MHzscyllo-Inositol treatment

TgCRND8 mice were administered *scyllo*-inositol (kind gift of Transition Therapeutics Inc.) *ad libitum* via drinking water at 10 mg/ml for 4 weeks starting at 5 months of age (McLaurinet al., 2006). The amount of water consumed was monitored across the cages to ensure similar dosage of *scyllo*-Inositol amongst animals.

8.3. Aβ plaque quantification

For the brighfield staining of Aβ plaques, sections were pretreated in 1% hydrogen peroxide and 70% formic acid. Aβ plaques were stained using 6F3D anti-Aβ antibody (1:400; Dako) followed by streptavidin-conjugated horseradish peroxidase (Vectastain ABC Kit, Vector Laboratories, Inc.) and 3,3′diaminobenzidine (DAB; Vector Laboratories, Inc.). Images were acquired at 4X on the Zeiss Axioplan II microscope, using Stereo Investigator (version 8.27, MBF Bioscience), and counted manually using ImageJ. Six coronal sections equally spanning the mouse brain (0.8 mm apart) were analzyed per mouse (Bregma +2 mm to Bregma −2.8 mm).

8.4. Quantification of astrocytes

Fluorescent detection of astrocytes was performed using rabbit anti-Glial Fibrillary Acidic Protein (GFAP) 1°antibody (1:500; Dako), and visualized using Alexafluor 647 donkey anti-Rabbit (1:200; Life Technologies) 2° antibody. Astrocytosis was assessed using the percentage area coverage of either the cortex or the hippocampus. Whole coronal section images were acquired at 10× on the ApoTome microscope (AxioImage M2; Carl Zeiss, Toronto, ON, Canada). Using ImageJ, the cortex or hippocampus was outlined manually with the outline tool and the total area (TA) was measured. The image was then converted using the "Binary" function, to select for stained astrocytes, and the area of the region of interest was again measured (RA). The RA value represents the area of immunofluorescent signal in the outlined area of interest. These two area values were then used to determine the percentage covered by astrocytes based on the following formula: RA/TA∗100.

8.5. Quantification of microglia

Microglial recruitment and Aβ engulfment were examined through fluorescent double staining of microglia and Aβ. Sections were pretreated with 10 mM citric acid buffer and heated for 30 min at 90°C. Detection of Aβ was performed with Thioflavin-S (ThioS; 1% in ddH_2O, Sigma), microglia with 1° Rabbit anti-Iba1 (1:500; Wako), and subsequently visualized with 2° Alexafluor 647 Donkey anti-Rabbit (1:200; Life Technologies) respectively. Co-localization of microglia with Aβ plaques was detected with a Zeiss spinning disk microscope (CSU-W1; Yokogawa Electric, Zeiss Axio Observer. Z1 – Carl Zeiss, Don Mills, Ontario, Canada) coupled to Axiocam camera and operated with Zen 1.1.2 software. Z-stack images (0.28 μm optimal slice thickness) were taken at 63x oil-immersion of plaques and the surrounding microglial cell population. Confocal z-stack images were reconstructed in three dimensions using Imaris software (Bitplane). The surface function was used to create three-dimensional surfaces of Aβ plaques and microglia (surface area detail level = 0.3 μm, threshold = 80) within each image. Using previously established methods, a surface was created for microglia fluorescence (Alexafluor 647 channel) and Aβ fluorescence (Alexafluor 488 channel) in the Imaris program (Jordão et al., 2013). These surfaces automatically generate 3D quantification of parameters such as microglia volume. To detect the Aβ within microglial cells, a separate channel was created by subtracting the ThioS staining for Aβ plaque from the image, representing the engulfed Aβ. Then, only staining that co-localized with Alexafluor 647 channel was isolated, and a new surface was created for the phagocytosed Aβ (surface area detail level = 0.3 μm, t hreshold = 80). Finally, the surface area of the microglia surrounding the Aβ plaque was also examined to determine whether treatment affected the recruitment of microglia.

8.6. Statistical analysis

Statistical analyses were performed using GraphPad Prism 6.0 (GraphPad Software Inc.). One-way ANOVA analyses with Tukey's multiple comparisons test, $\alpha = 0.05$, was used to examine differences between combination treatment, *scyllo*-inositol treatment and untreated transgenic mice.

Ethical approval and consent

This study received local approval from the Animal Care Committee of the Sunnybrook Health Sciences Center, which adheres to the Policies and Guidelines of the Canadian Council on Animal Care and meets all the requirements of the Provincial Statute of Ontario, Animals for Research Act as well as those of the Federal Health of Animals Act.

Funding sources

The authors would like to acknowledge the following funding agencies: CIHR (JM PRG 37857; IA MOP 93603). The National Institutes of Health under Grant No. R01-EB003268, as well as the Canada Research Chair Program (KH).

Acknowledgements

We would like to thank Transition Therapeutics Inc. for the kind gift of *scyllo*-inositol and Shawna Rideout for her help with animal care.

References

Ahmed, M., Davis, J., Aucoin, D., Sato, T., Ahuja, S., Aimoto, S., Elliott, J.I., Van Nostrand, W.E., Smith, S.O., 2010. Structural conversion of neurotoxic amyloidβ 1–42 oligomers to fibrils. Nat. Struct. Mol. Biol. 17, 561–567. https://doi.org/10.1038/nsmb.1799.

Alecou, T., Giannakou, M., Damianou, C., 2017. Amyloid β plaque reduction with antibodies crossing the blood-brain barrier, which was opened in 3 sessions of focused ultrasound in a rabbit model. J. Ultrasound Med. 36, 2257–2270. https://doi.org/10.1002/jum.14256.

Aytan, N., Choi, J.K., Carreras, I., Kowall, N.W., Jenkins, B.G., Dedeoglu, A., 2013. Combination therapy in a transgenic model of Alzheimer's disease. Exp. Neurol. 250, 228–238. https://doi.org/10.1016/j.expneurol.2013.10.001.

Banks, W.A., Terrell, B., Farr, S.A., Robinson, S.M., Nonaka, N., Morley, J.E., 2002. Passage of amyloid β protein antibody across the blood–brain barrier in a mouse model of Alzheimer's disease. Peptides 23, 2223–2226. https://doi.org/10.1016/S0196-9781(02)00261-9.

Bard, F., Barbour, R., Cannon, C., Carretto, R., Fox, M., Games, D., Guido, T., Hoenow, K., Hu, K., Johnson-wood, K., Khan, K., Kholodenko, D., Lee, C., Lee, M., Motter, R., Nguyen, M., Reed, A., Schenk, D., Tang, P., Vasquez, N., Seubert, P., Yednock, T., 2003. Epitope and isotype specificities of antibodies to β-amyloid peptide for protection against Alzheimer's disease-like neuropathology. Proc. Natl. Acad. Sci. U.S.A. 100, 2023–2028. https://doi.org/10.1073/pnas.0436286100.

Burgess, A., Ayala-Grosso, C.A., Ganguly, M., Jordão, J.F., Aubert, I., Hynynen, K., 2011. Targeted delivery of neural stem cells to the brain using MRI-guided focused ultrasound to disrupt the blood-brain barrier. PLoS One 6. https://doi.org/10.1371/journal.pone.0027877.

Burgess, A., Dubey, S., Yeung, S., Hough, O., Eterman, N., Aubert, I., Hynynen, K., 2014. Alzheimer disease in a mouse model: MR imaging-guided focused ultrasound targeted to the hippocampus opens the blood-brain barrier and improves pathologic abnormalities and behavior. Radiology 273, 736–745. https://doi.org/10.1148/radiol.14140245.

Chopra, R., Curiel, L., Staruch, R., Morrison, L., Hynynen, K., 2009. An MRI-compatible system for focused ultrasound experiments in small animal models. Med. Phys. 36, 1867–1874. https://doi.org/10.1118/1.3115680.

Condello, C., Yuan, P., Schain, A., Grutzendler, J., 2015. Microglia constitute a barrier that prevents neurotoxic protofibrillar Aβ42 hotspots around plaques. Nat. Commun. 6, 6176. https://doi.org/10.1038/ncomms7176.

Diaz, R.J., McVeigh, P.Z., O'Reilly, M.A., Burrell, K., Bebenek, M., Smith, C., Etame, A.B., Zadeh, G., Hynynen, K., Wilson, B.C., Rutka, J.T., 2014. Focused ultrasound delivery of Raman nanoparticles across the blood-brain barrier: potential for targeting experimental brain tumors. Nanomed. Nanotechnol. Biol. Med. 10, 1075–1087. https://doi.org/10.1016/j.nano.2013.12.006.

Doody, R.S., Thomas, R.G., Farlow, M., Iwatsubo, T., Vellas, B., Joffe, S., Kieburtz, K., Raman, R., Sun, X., Aisen, P.S., Siemers, E., Liu-Seifert, H., Mohs, R., 2014. Phase 3 trials of solanezumab for mild-to-moderate Alzheimer's disease. N. Engl. J. Med. 370, 311–321. https://doi.org/10.1056/NEJMoa1312889.

Ellens, N.P.K., Kobelevskiy, I., Chau, A., Waspe, A.C., Staruch, R.M., Chopra, R., Hynynen, K., 2015. The targeting accuracy of a preclinical MRI-guided focused ultrasound system. Med. Phys. 42, 430–439. https://doi.org/10.1118/1.4903950.

Fenili, D., Brown, M., Rappaport, R., McLaurin, J., 2007. Properties of *scyllo*-inositol as a therapeutic treatment of AD-like pathology. J. Mol. Med. 85, 603–611. https://doi.org/10.1007/s00109-007-0156-7.

Fenili, D., Weng, Y.Q., Aubert, I., Nitz, M., McLaurin, J., 2011. Sodium/*myo*-inositol transporters: Substrate transport requirements and regional brain expression in the TgCRND8 mouse model of amyloid pathology. PLoS One 6, 2–10. https://doi.org/10.1371/journal.pone.0024032.

Frenkel, D., Balass, M., Solomon, B., Ashall, F., Goate, A.M., Balass, M., Heldman, Y., Cabilly, S., Givol, D., Katchalski-Katzir, E., Fuchs, S., Barrow, C.J., Akikazu, Y., Kenny, P.T.M., Zagorski, M.G., Hanan-Aharon, E., Solomon, B., Levine, H., Maggio, J.E., Stimson, E.R., Ghilardi, J.R., Allen, C.J., Dahl, C.E., Whitcomb, D.C., Vigna, S.R., Vinters, H.V., Labenski, M.E., Mantyh, P.W., Medynski, D., Scott, J.K., Smith, G.P., Selkoe, D.J., Solomon, B., Koppel, R., Frenkel, D., Hanan-Aharon, E., Soto, C., Kindy, M.S., Baumann, M., Frangione, B., 1998. N-terminal EFRH sequence of

Alzheimer's β-amyloid peptide represents the epitope of its anti-aggregating antibodies. J. Neuroimmunol. 88, 85–90. https://doi.org/10.1016/S0165-5728(98)00098-8.

Hardy, J., Selkoe, D.J., 2002. The amyloid hypothesis of Alzheimer's disease: progress and problems on the road to therapeutics. Science 297, 353–356. https://doi.org/10.1126/science.1072994.

Hawkes, C.A., Deng, L., Fenili, D., Nitz, M., McLaurin, J., 2012. In vivo uptake of β-amyloid by non-plaque associated microglia. Curr. Alzheimer Res. 9, 890–901. https://doi.org/10.2174/156720512803251084.

Hawkes, C.A., Deng, L.H., Shaw, J.E., Nitz, M., McLaurin, J., 2010. Small molecule β-amyloid inhibitors that stabilize protofibrillar structures in vitro improve cognition and pathology in a mouse model of Alzheimer's disease. Eur. J. Neurosci. 31, 203–213. https://doi.org/10.1111/j.1460-9568.2009.07052.x.

Hynynen, K., 2010. MRI-guided focused ultrasound treatments. Ultrasonics 50, 221–229. https://doi.org/10.1016/j.ultras.2009.08.015.

Hynynen, K., McDannold, N., Vykhodtseva, N., Jolesz, F.A., 2001. Noninvasive MR imaging–guided focal opening of the blood-brain barrier in rabbits. Radiology 220, 640–646. https://doi.org/10.1148/radiol.2202001804.

Hynynen, K., McDannold, N., Vykhodtseva, N., Raymond, S., Weissleder, R., Jolesz, F. A, Sheikov, N., 2006. Focal disruption of the blood–brain barrier due to 260-kHz ultrasound bursts: a method for molecular imaging and targeted drug delivery. J. Neurosurg. 105, 445–454. https://doi.org/10.3171/jns.2006.105.3.445.

Jordão, J.F., Ayala-Grosso, C.A., Markham, K., Huang, Y., Chopra, R., McLaurin, J., Hynynen, K., Aubert, I., 2010. Antibodies targeted to the brain with image-guided focused ultrasound reduces amyloid-β plaque load in the TgCRND8 mouse model of Alzheimer's disease. PLoS One 5, e10549. https://doi.org/10.1371/journal.pone.0010549.

Jordão, J.F., Thévenot, E., Markham-Coultes, K., Scarcelli, T., Weng, Y.-Q., Xhima, K., O'Reilly, M., Huang, Y., McLaurin, J., Hynynen, K., Aubert, I., 2013. Amyloid-β plaque reduction, endogenous antibody delivery and glial activation by brain-targeted, transcranial focused ultrasound. Exp. Neurol. 248, 16–29. https://doi.org/10.1016/j.expneurol.2013.05.008.

Kotilinek, L.A., Bacskai, B., Westerman, M., Kawarabayashi, T., Younkin, L., Hyman, B. T., Younkin, S., Ashe, K.H., 2002. Reversible memory loss in a mouse transgenic model of Alzheimer's disease. J. Neurosci. 22, 6331–6335. 20026675.

Lai, A.Y., McLaurin, J., 2012. Clearance of amyloid-β peptides by microglia and macrophages: the issue of what, when and where. Future Neurol. 7, 165–176. https://doi.org/10.2217/fnl.12.6.

Leinenga, G., Gotz, J., 2015. Scanning ultrasound removes amyloid-β and restores memory in an Alzheimer's disease mouse model. Sci. Transl. Med. 7. https://doi.org/10.1126/scitranslmed.aaa2512.

Liu, Z., Zhang, A., Sun, H., Han, Y., Kong, L., Wang, X., 2017. Two decades of new drug discovery and development for Alzheimer's disease. RSC Adv. 7, 6046–6058. https://doi.org/10.1039/c6ra26737h.

Ma, K., Thomason, L.A.M., McLaurin, J., 2012. scyllo-Inositol, preclinical, and clinical data for Alzheimer's Disease. Adv. Pharmacol. https://doi.org/10.1016/B978-0-12-394816-8.00006-4.

McLaurin, J., Cecal, R., Kierstead, M.E., Tian, X., Phinney, A.L., Manea, M., French, J.E., Lambermon, M.H.L., Darabie, A.A., Brown, M.E., Janus, C., Chishti, M.A., Horne, P., Westaway, D., Fraser, P.E., Mount, H.T.J., Przybylski, M., St George-Hyslop, P., 2002. Therapeutically effective antibodies against amyloid-β peptide target amyloid-β residues 4–10 and inhibit cytotoxicity and fibrillogenesis. Nat. Med. 8, 1263–1269. https://doi.org/10.1038/nm790.

McLaurin, J., Golomb, R., Jurewicz, A., Antel, J.P., Fraser, P.E., 2000. Inositol Stereoisomers Stabilize an Oligomeric Aggregate of Alzheimer Amyloid β Peptide and Inhibit Aβ-induced Toxicity. J. Biol. Chem. 275, 18495–18502. https://doi.org/10.1074/jbc.M906994199.

McLaurin, J., Kierstead, M.E., Brown, M.E., Hawkes, C.A., Lambermon, M.H.L., Phinney, A.L., Darabie, A.A., Cousins, J.E., French, J.E., Lan, M.F., Chen, F., Wong, S.S.N., Mount, H.T.J., Fraser, P.E., Westaway, D., George-Hyslop, P.S., 2006. Cyclohexanehexol inhibitors of Abeta aggregation prevent and reverse Alzheimer phenotype in a mouse model. Nat. Med. 12, 801–808. https://doi.org/10.1038/nm1423.

Meng, Y., Volpini, M., Black, S., Lozano, A.M., Hynynen, K., Lipsman, N., 2017. Focused ultrasound as a novel strategy for Alzheimer's disease therapeutics. Ann. Neurol. 81, 1–7. https://doi.org/10.1002/ana.24933.

Morgan, D., Gitter, B.D., 2004. Evidence supporting a role for anti-Abeta antibodies in the treatment of Alzheimer's disease. Neurobiol. Aging 25, 605–608. https://doi.org/10.1016/j.neurobiolaging.2004.02.005.

Nie, Q., Du, X., Geng, M., 2011. Small molecule inhibitors of amyloid β peptide aggregation as a potential therapeutic strategy for Alzheimer's disease. Acta Pharmacol. Sin. 32, 545–551. https://doi.org/10.1038/aps.2011.14.

O'Reilly, M.A., Hynynen, K., 2012. Blood-brain barrier: real-time feedback-controlled focused ultrasound disruption by using an acoustic emissions-based controller. Radiology 263, 96–106. https://doi.org/10.1148/radiol.11111417.

Pekny, M., Pekna, M., Messing, A., Steinhäuser, C., Lee, J.M., Parpura, V., Hol, E.M., Sofroniew, M.V., Verkhratsky, A., 2016. Astrocytes: a central element in neurological diseases. Acta Neuropathol. 131, 323–345. https://doi.org/10.1007/s00401-015-1513-1.

Reitz, C., Mayeux, R., 2014. Alzheimer disease: epidemiology, diagnostic criteria, risk factors and biomarkers. Biochem. Pharmacol. 88, 640–651. https://doi.org/10.1016/j.bcp.2013.12.024.

Rodriguez, J., Olabarria, M., Rodríguez, J.J., Olabarria, M., Chvatal, A., Verkhratsky, A., 2009. Astroglia in dementia and Alzheimer's disease. Cell Death Differ. 16, 378–385. https://doi.org/10.1038/cdd.2008.172.

Salloway, S., Sperling, R., Keren, R., Porsteinsson, A.P., Van Dyck, C.H., Tariot, P.N., Gilman, S., Arnold, D., Abushakra, S., Hernandez, C., Crans, G., 2011. A phase 2 randomized trial of ELND005, *scyllo*-inositol, in mild to moderate Alzheimer disease. Neurology 77, 1253–1262. https://doi.org/10.1212/WNL.0b013e3182309fa5.

Salloway, S., Sperling, R., Fox, N.C., Blennow, K., Klunk, W., Raskind, M., Sabbagh, M., Honig, L.S., Porsteinsson, A.P., Ferris, S., Reichert, M., Ketter, N., Nejadnik, B., Guenzler, V., Miloslavsky, M., Wang, D., Lu, Y., Lull, J., Tudor, I.C., Liu, E., Grundman, M., Yuen, E., Black, R., Brashear, H.R., 2014. Two phase 3 trials of bapineuzumab in mild-to-moderate Alzheimer's disease. N. Engl. J. Med. 370, 322–333. https://doi.org/10.1056/NEJMoa1304839.

Selkoe, D.J., 2001. Alzheimer's Disease: Genes, Proteins, and Therapy. Physiol. Reviews 81, 741–767. https://doi.org/10.1016/0092-8674(88)90462-x.

Sheikov, N., McDannold, N., Sharma, S., Hynynen, K., 2008. Effect of focused ultrasound applied with an ultrasound contrast agent on the tight junctional integrity of the brain microvascular endothelium. Ultrasound Med. Biol. 34, 1093–1104. https://doi.org/10.1016/j.ultrasmedbio.2007.12.015.

Sheikov, N., McDannold, N., Vykhodtseva, N., Jolesz, F., Hynynen, K., 2004. Cellular mechanisms of the blood-brain barrier opening induced by ultrasound in presence of microbubbles. Ultrasound Med. Biol. 30, 979–989. https://doi.org/10.1016/j.ultrasmedbio.2004.04.010.

Tarasoff-Conway, J.M., Carare, R.O., Osorio, R.S., Glodzik, L., Butler, T., Fieremans, E., Axel, L., Rusinek, H., Nicholson, C., Zlokovic, B.V., Frangione, B., Blennow, K., Ménard, J., Zetterberg, H., Wisniewski, T., de Leon, M.J., 2015. Clearance systems in the brain-implications for Alzheimer disease. Nat. Rev. Neurol. 11, 457–470. https://doi.org/10.1038/nrneurol.2015.119.

Thévenot, E., Jordão, J.F., O'Reilly, M.A., Markham, K., Weng, Y.Q., Foust, K.D., Kaspar, B.K., Hynynen, K., Aubert, I., 2012. Targeted delivery of self-complementary adeno-associated virus Serotype 9 to the brain, using magnetic resonance imaging-guided focused ultrasound. Hum. Gene Ther. 23, 1144–1155. https://doi.org/10.1089/hum.2012.013.

Weiner, H.L., Frenkel, D., 2006. Immunology and immunotherapy of Alzheimer's disease. Nat. Rev. Immunol. 6, 404–416. https://doi.org/10.1038/nri1881.